Chaperone-enhanced purification of unconventional myosin 15, a molecular motor specialized for stereocilia protein trafficking

Jonathan E. Bird[a], Yasuharu Takagi[b], Neil Billington[b], Marie-Paule Strub[c], James R. Sellers[b,1], and Thomas B. Friedman[a,1]

[a]Laboratory of Molecular Genetics, National Institute on Deafness and Other Communication Disorders, and [b]Laboratory of Molecular Physiology and [c]Biochemistry and Biophysics Center, National Heart, Lung, and Blood Institute, National Institutes of Health, Bethesda, MD 20892

Edited by James A. Spudich, Stanford University School of Medicine, Stanford, CA, and approved July 16, 2014 (received for review May 21, 2014)

Unconventional myosin 15 is a molecular motor expressed in inner ear hair cells that transports protein cargos within developing mechanosensory stereocilia. Mutations of myosin 15 cause profound hearing loss in humans and mice; however, the properties of this motor and its regulation within the stereocilia organelle are unknown. To address these questions, we expressed a subfragment 1-like (S1) truncation of mouse myosin 15, comprising the predicted motor domain plus three light-chain binding sites. Following unsuccessful attempts to express functional myosin 15-S1 using the *Spodoptera frugiperda* (Sf9)-baculovirus system, we discovered that coexpression of the muscle-myosin–specific chaperone UNC45B, in addition to the chaperone heat-shock protein 90 (HSP90) significantly increased the yield of functional protein. Surprisingly, myosin 15-S1 did not bind calmodulin with high affinity. Instead, the IQ domains bound essential and regulatory light chains that are normally associated with class II myosins. We show that myosin 15-S1 is a barbed-end–directed motor that moves actin filaments in a gliding assay (~430 nm·s^{-1} at 30 °C), using a power stroke of 7.9 nm. The maximum ATPase rate (k_{cat} ~6 s^{-1}) was similar to the actin-detachment rate (k_{det} = 6.2 s^{-1}) determined in single molecule optical trapping experiments, indicating that myosin 15-S1 was rate limited by transit through strongly actin-bound states, similar to other processive myosin motors. Our data further indicate that in addition to folding muscle myosin, UNC45B facilitates maturation of an unconventional myosin. We speculate that chaperone coexpression may be a simple method to optimize the purification of other myosin motors from Sf9 insect cells.

deafness | DFNB3 | myosin XV | UNC-45

Unconventional myosin 15 is expressed by inner ear hair cells and accumulates at the tips of mechanosensory stereocilia (1, 2), actin-based organelles that are stimulated by sound and accelerations. A missense substitution in the myosin 15 motor domain results in abnormally short stereocilia in the *Myo15*$^{sh2/sh2}$ (shaker 2) mouse, indicating that myosin 15 motor activity is essential for elongation of the core actin filaments during development (1, 3). Emphasizing the critical importance of myosin 15 for sensory function, mutations of the orthologous *MYO15A* also cause profound nonsyndromic autosomal recessive deafness (DFNB3) in humans (4, 5). Myosin 15 is hypothesized to be a molecular motor that transports the scaffolding protein whirlin (DFNB31) and epidermal growth factor receptor kinase substrate 8 (EPS8) to the stereocilia tips, where these cargos regulate elongation of the developing actin core (6, 7). Although myosin 15 motility has not been visualized in live hair cells, it similarly transports whirlin and EPS8 to the tips of filopodia, finger-like protrusions of bundled actin filaments (6, 7). Little is known about the functional properties of myosin 15, its mechanism of motility along stereocilia or filopodial actin filaments, or how this might be altered by mutations associated with DFNB3 human deafness.

Myosins are a superfamily of actin-activated P-loop ATPases that produce force to power fundamental cellular processes, such as cytokinesis and vesicle trafficking (8). Biochemical and biophysical analyses of purified isozymes have been critical to deciphering their cellular functions. Most myosins share a common catalytic mechanism, but kinetic tuning of reaction rates can result in very different characteristics (9, 10). An important property is the duty ratio; defined as the fraction of the ATPase cycle that myosin spends strongly bound to actin. Low-duty ratio motors, exemplified by muscle myosins, spend a small fraction (~0.05) of their cycle strongly bound to actin and act in large ensembles. In contrast, processive motors like myosin 5a have a duty ratio of >0.7 at saturating [actin], and thus spend most of their ATPase cycle in strongly actin-bound states (11). For myosin 5a, the high-duty ratio supports the processive movement of dimers by increasing the likelihood that one head is always bound to actin, thus preventing diffusion away from the filament track.

Myosin 15 is the largest myosin heavy chain in the mammalian proteome and is highly expressed in the inner ear and endocrine organs (2). Phylogenetic analysis of motor domain sequences reveals its close relationship with unconventional class VII and X myosins, in addition to sharing similar myosin tail homology 4 (MyTH4), Src homology 3 (SH3) and band 4.1, ezrin, radixin, moesin (FERM) domains in the C-terminal tail (Fig. 1*A*). Alternate splicing of exon 2 (1, 2), creates two protein isoforms that are identical except for a large (133 kDa) proline-rich N-terminal extension that is unique

Significance

Mutations in unconventional myosin 15 cause nonsyndromic autosomal recessive deafness, a common form of hereditary hearing loss in humans. Myosin 15 is required for the development of hair cell mechanosensory stereocilia that detect sounds within the inner ear. To our knowledge, our work offers the first insight into the biophysical properties of purified myosin 15. Using ensemble and single molecule techniques, we show that myosin 15 is a high-duty ratio motor, which is a characteristic of myosins that can move processively along actin filaments. We also introduce a new strategy for producing myosins by chaperone coexpression in *Spodoptera frugiperda* insect cells. This approach may help optimize expression of skeletal and cardiac muscle myosins, which are emerging as translational drug targets but are presently refractory to larger-scale purification.

Author contributions: J.E.B., Y.T., N.B., J.R.S., and T.B.F. designed research; J.E.B., Y.T., and N.B. performed research; J.E.B. and M.-P.S. contributed new reagents/analytic tools; J.E.B., Y.T., and N.B. analyzed data; J.E.B. conceived technique of chaperone coexpression; and J.E.B., Y.T., N.B., M.-P.S., J.R.S., and T.B.F. wrote the paper.

The authors declare no conflict of interest.

This article is a PNAS Direct Submission.

Freely available online through the PNAS open access option.

[1]To whom correspondence may be addressed. Email: friedman@nidcd.nih.gov or sellersj@nhlbi.nih.gov.

This article contains supporting information online at www.pnas.org/lookup/suppl/doi:10.1073/pnas.1409459111/-/DCSupplemental.

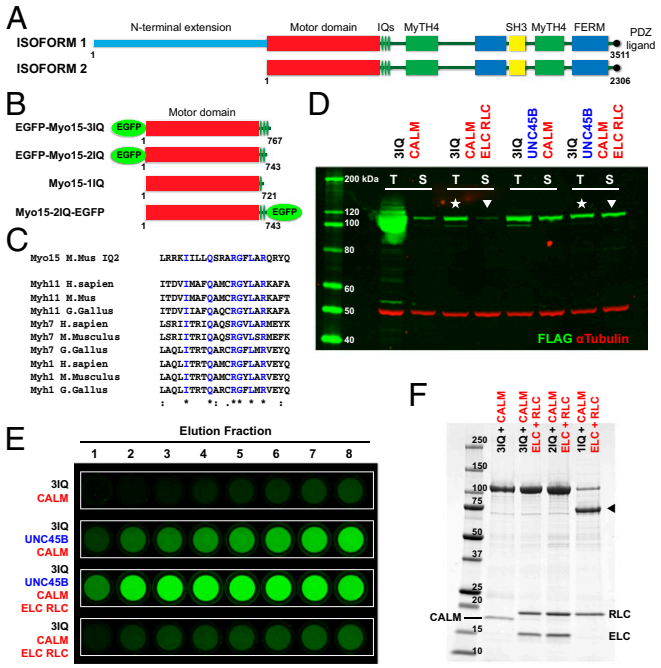

Fig. 1. Purification of mouse myosin 15 from Sf9 cells by chaperone coexpression. (*A*) Schematic domain structure of mouse myosin 15 isoforms. (*B*) Motor domain constructs used in this study. All expressed proteins have a C-terminal FLAG epitope for affinity purification. (*C*) ClustalW alignments of the second IQ of myosin 15 show similarity to the ELC binding site (first IQ) of class II myosins. (*D*) Coexpression with UNC45B/HSP90AA1 increases the solubility of EGFP-Myo15-3IQ in Sf9 insect cells (abbreviated to 3IQ for *D*–*F*). Western blot probed with antibody against FLAG (green) and alpha-tubulin (red). Total and soluble fractions were prepared from equal volumes of Sf9 cell cultures expressing EGFP-Myo15-3IQ, plus combinations of chaperones and light chains as shown. EGFP-Myo15-3IQ sedimented when coexpressed with calmodulin (CALM) alone, or with CALM + ELC + RLC. Expression of UNC45B + HSP90AA1 increased EGFP-Myo15-3IQ in the supernatant (compare arrowheads), but did not change heavy chain expression overall (compare stars). (*E*) Supernatants from *D* were bound to FLAG-M2 affinity resin, eluted with FLAG peptide (0.5-mL fractions), and assayed for EGFP fluorescence (representative of three experiments). Individual images (outlined in white) for each condition were captured with identical settings and consolidated. Samples coexpressing RLC + ELC in addition to UNC45B + HSP90AA1 eluted in earlier fractions (third row), compared with coexpressing UNC45B/HSP90AA1 and CALM (second row). (*F*) SDS/PAGE of FLAG-purified proteins from Sf9 cells expressing UNC45B + HSP90AA1 and combinations of Myo15 IQ mutants and lights chains as indicated. Note increased mobility of Myo15-1IQ (arrowhead) without an EGFP fusion.

to isoform 1 (Fig. 1*A*). The function of isoform 1 is unknown, whereas isoform 2 targets to stereocilia and filopodia tips, and is sufficient to rescue stereocilia development in *Myo15*$^{sh2/sh2}$ hair cells (1, 6). Myosin 15 has three presumed light-chain binding sites (IQ motifs) that are predicted to form a lever arm; however, the light chains that potentially bind these in vivo are unknown.

To understand how myosin 15 operates within the stereocilia organelle, we have purified the motor domain and used a combination of single molecule and ensemble kinetic/mechanical analyses to determine its properties. While attempting to purify myosin 15 from *Spodoptera frugiperda* (Sf9) insect cells, we discovered that coexpression of heat-shock protein 90 (HSP90) and its cochaperone UNC45B significantly improved the yield of soluble protein. We demonstrate that purified myosin 15 is a mechanically active, barbed-end–directed molecular motor that exhibits a high-duty ratio. These data suggest that myosin 15 might be capable of processive motility if dimerized, consistent with its proposed role as a stereocilia transporter.

Results

Myosin 15 Requires the UNC45B and HSP90AA1 Chaperones to Fold in Sf9 Cells. Because myosin 15 is not abundantly expressed throughout the body (2), we attempted to purify a recombinant enzyme from baculovirus-infected Sf9 insect cells, an approach that has been successful with other myosins. We engineered a recombinant baculovirus expression construct consisting of the myosin 15 motor domain and the three predicted IQ motifs (Fig. 1*B*), fused at the N terminus to enhanced green fluorescent protein (EGFP) and a C-terminal FLAG epitope to aid purification. EGFP-Myo15-3IQ was coexpressed with calmodulin, which is a light chain that binds IQ motifs. EGFP-Myo15-3IQ was highly expressed in Sf9 cells, however immunoblotting revealed that the majority of protein in cell lysates sedimented (48 $kG_{max} \times 30$ min), indicating that it was heavily aggregated (Fig. 1*D*). EGFP-Myo15-3IQ remaining in the soluble fraction was incubated with a FLAG-M2 affinity matrix, but only trace quantities of protein could be eluted using FLAG peptide (Fig. 1*E*, first row).

We hypothesized that EGFP-Myo15-3IQ might require additional factors to fold correctly within the Sf9 cell. An intriguing candidate was UNC-45, a member of the UNC-45/Cro1/She4 (UCS) domain-containing family, which can bind conventional class II muscle myosin and promote HSP90-dependent folding (12, 13). We generated a baculovirus expressing both mouse UNC45B and mouse HSP90AA1 and confirmed that both proteins were expressed at their anticipated molecular weights (Fig. S1*A*). Although HSP90 is expressed endogenously, no UNC45B was detected in uninfected Sf9 cells (Fig. S1*A*). When EGFP-Myo15-3IQ was coexpressed with UNC45B, HSP90AA1, and calmodulin in Sf9 cells, we observed an increase of both soluble EGFP-Myo15-3IQ (Fig. 1*D*), and also protein eluting from the FLAG-M2 affinity matrix (Fig. 1*E*, second row). However, the purified protein eluted in a shallow gradient from the affinity matrix and was visibly turbid, suggesting it was likely aggregated.

Hydrophobic residues within IQ motifs are known to promote myosin aggregation if solvent exposed. Although calmodulin did copurify with EGFP-Myo15-3IQ (Fig. 1*F*), we hypothesized this was not sufficient to occupy all three IQ motifs. We examined alignments with other myosin light-chain binding sites and noted similarity between the second IQ motif of myosin 15 and the first IQ of vertebrate myosin 2 (Fig. 1*C*), which associates with the essential light chain (14). We next expressed EGFP-Myo15-3IQ with essential (ELC) and regulatory (RLC) light chains from smooth muscle, in addition to UNC45B, HSP90AA1, and calmodulin as before. EGFP-Myo15-3IQ now remained soluble following the centrifugal clearing step (Fig. 1*D*), eluted in significantly earlier fractions from the FLAG-M2 matrix (Fig. 1*E*, third row), and was no longer turbid. To test if ELC and RLC alone were sufficient to increase the yield of EGFP-Myo15-3IQ purified from Sf9 cells, we repeated the purification in the absence of the UNC45B and HSP90AA1 chaperone virus. The majority of EGFP-Myo15-3IQ again sedimented (Fig. 1*D*) and only trace quantities eluted from the FLAG-M2 matrix (Fig. 1*E*, fourth row). These results were similar to coexpressing EGFP-Myo15-3IQ with calmodulin alone (Fig. 1 *D* and *E*) and indicated that the increased yields were a specific effect of overexpressing UNC45B and HSP90AA1.

We considered whether UNC45B and HSP90AA1 might increase the yield of EGFP-Myo15-3IQ indirectly, by competing for cellular resources and lowering heavy chain expression to a level that could fold correctly. This interpretation was not supported by our experimental data. The total cell expression level of EGFP-Myo15-3IQ when coexpressed with ELC, RLC, and calmodulin did not significantly change when the virus encoding UNC45B and HSP90AA1 was added (Fig. 1*D*, stars). However, despite comparable total expression levels, there was an increase in soluble EGFP-Myo15-3IQ detected in the supernatant (Fig. 1*D*, arrowheads) and

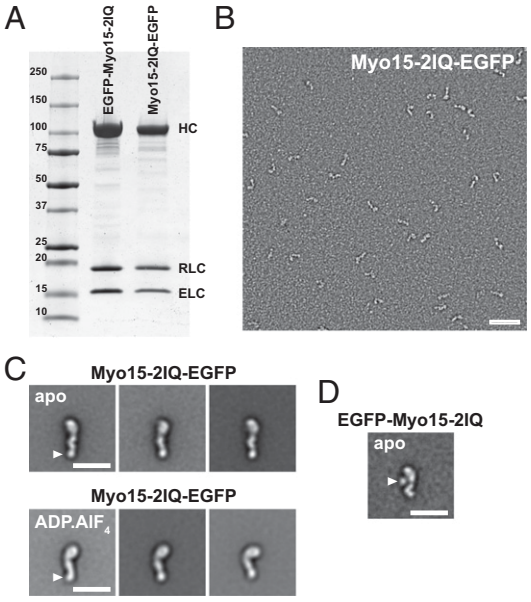

Fig. 2. Chaperone-purified myosin 15 is correctly folded and the lever arm fully occupied by ELC and RLC. (*A*) Representative Coomassie-stained SDS/PAGE gel of EGFP-Myo15-2IQ and Myo15-2IQ-EGFP after large-scale expression and purification by ion exchange and size exclusion chromatography. The identity of the myosin 15 heavy chain (HC), RLC, and ELC were confirmed by LC-MS/MS sequencing. (*B*) Representative raw TEM micrograph of negative-stained Myo15-2IQ-EGFP. (Scale bar, 50 nm.) (*C*) Class averages of Myo15-2IQ-EGFP with no-nucleotide (apo) or with ADP·AlF_4 bound shows postpower stroke- (rigor) and prepower stroke-like states, respectively. The globular EGFP moiety is visible (arrowhead) at the C terminus. (Scale bars, 20 nm.) (*D*) Class average of EGFP-Myo15-2IQ (N-terminal EGFP fusion) under no-nucleotide (apo) conditions. (Scale bar, 20 nm.) Note the altered position of the EGFP moiety (arrowhead).

also eluting from the FLAG-M2 matrix (Fig. 1*E*, compare third and fourth rows) when UNC45B and HSP90AA1 were present. Thus, reduced expression of the heavy chain did not explain the increased yield of EGFP-Myo15-3IQ. Consistent with a specific role in polypeptide maturation, we detected small quantities of UNC45B that copurified with EGFP-Myo15-3IQ from the FLAG-M2 matrix (Fig. S1*B*). These data indicate that UNC45B could stably bind a subpopulation of EGFP-Myo15-3IQ molecules and suggest that EGFP-Myo15-3IQ is a client for the UNC-45/HSP90 chaperone complex.

Myosin 15 Binds Essential and Regulatory Light Chains in Preference to Calmodulin. Since the coexpression of ELC and RLC appeared to prevent aggregation of EGFP-Myo15-3IQ bound to calmodulin (Fig. 1*E*), we investigated light chain binding in more detail. EGFP-Myo15-3IQ was expressed with UNC45B, HSP90AA1, along with ELC, RLC, and calmodulin. Under these conditions, both ELC and RLC coeluted with EGFP-Myo15-3IQ (Fig. 1*F*, second lane) in an ∼1:1 stoichiometry. Note that the RLC binds dye more intensely than ELC (15). Trace quantities of calmodulin were still detected, suggesting that this light chain was competing with ELC and/or RLC for a common binding site (Fig. 1*F*). Truncations of the myosin 15 IQ domains were used to explore the configuration of ELC and RLC binding. ELC and RLC bound to the first two IQs domains, because EGFP-Myo15-2IQ (Fig. 1*B*) coeluted with ELC and RLC in similar relative ratios as observed for EGFP-Myo15-3IQ (Fig. 1*F*). These data further indicated that the third predicted IQ domain was unoccupied. Only RLC copurified with Myo15-1IQ, confirming that RLC bound the first IQ domain and that ELC was associated with the second IQ domain (Fig. 1*F*). There were no traces of calmodulin coeluting with Myo15-1IQ, showing that calmodulin competed with ELC for binding to the second IQ. We conclude that ELC and RLC bind to myosin 15 in a structurally reverse order compared with myosin 2 (14), consistent with the predictions from sequence alignments (Fig. 1*C*).

Chaperone-Purified Myosin 15 Is Correctly Folded. We next examined the structure of purified myosin 15 to determine if it was correctly folded. To avoid potential aggregation through a solvent-exposed third IQ domain, we used 2IQ truncations bound to ELC and RLC for all further studies (Fig. 1*B*). Scaling up of expression and further purification by anion exchange and size exclusion chromatography, yielded 2–3 mg of EGFP-Myo15-2IQ per 1 L culture of 2×10^9 Sf9 cells (Fig. 2*A*). Using identical techniques, we also generated a C-terminal–tagged EGFP fusion (Myo15-2IQ-EGFP) to facilitate gliding filament and optical trapping experiments (Fig. 2*A*).

Negative-stain transmission electron microscopy (TEM) was used to examine the macromolecular structure of purified Myo15-2IQ-EGFP molecules (Fig. 2*B*). Single molecule class averaging under nucleotide-free (apo) conditions confirmed that Myo15-2IQ-EGFP had both a clearly defined globular head domain, in addition to a lever arm (formed of IQ motifs) that was fully occupied by the ELC and RLC light chains (Fig. 2*C*). Similar observations were made for EGFP-Myo15-2IQ, except for the altered position of the N-terminal EGFP moiety (Fig. 1*D*). Incubation of Myo15-2IQ-EGFP with ADP·AlF_4 was accompanied by rotation of the lever arm, a conformation that is consistent with formation of a prepower stroke like state (Fig. 1*C*). These data demonstrate that both EGFP-Myo15-2IQ and Myo15-2IQ-EGFP purified from Sf9 cells were monomeric and had conformations expected for a myosin motor with two light chains bound to the lever arm.

Steady-State Activation of the Myosin 15 ATPase by Actin Filaments. To determine if EGFP-Myo15-2IQ purified using chaperone coexpression was catalytically active, we measured ATP hydrolysis using an enzyme-linked NADH assay to detect the steady-state production of ADP (Fig. 3*A*). In the absence of actin filaments, the basal steady-state ATPase activity was 0.09 ± 0.02 s^{-1} (SEM) assayed with 100 mM KCl at 20 °C. ATPase activity was maximally activated 67-fold by the addition of actin to an extrapolated maximal rate (k_{cat}) of 6.0 ± 0.5 s^{-1} (SEM). Half-maximal activation occurred (K_{ATPase}) at 164.5 ± 18.9 μM actin (SEM), indicating a weak apparent affinity for actin under these assay conditions. Because the K_{ATPase} was in excess of the highest [actin] assayed, we repeated these measurements under reduced salt concentration in an attempt to increase the apparent affinity for actin and establish the maximal rate with a higher certainty. The K_{ATPase} reduced with decreasing salt concentration, whereas k_{cat} remained constant at ∼6 s^{-1}; all data are mean ± SEM, (10 mM KCl) k_{cat} = 5.5 ± 0.1 s^{-1}, K_{ATPase} = 13.1 ± 0.9 μM; (25 mM KCl) k_{cat} = 5.7 ± 0.1 s^{-1}, K_{ATPase} = 22.8 ± 0.8 μM; (50 mM KCl) k_{cat} = 6.0 ± 0.3 s^{-1}, K_{ATPase} = 49.9 ± 4.1 μM (Fig. 3*A*). The basal activity was unaffected by salt concentration (0.08–0.09 s^{-1}).

Myosin 15 Is a Barbed-End Directed Motor. We next examined if purified myosin 15 was mechanically active and able to move fluorescently labeled actin filaments in a gliding assay (16, 17). Nonspecific adsorption of EGFP-Myo15-2IQ to the coverglass using nitrocellulose did not support motility, likely due to the small, compact nature of the myosin head domain. Instead, when Myo15-2IQ-EGFP was stereo-specifically adsorbed with anti-EGFP antibodies, robust actin filament motility was observed at 30 °C. The average filament velocity was 429 ± 74 nm·s^{-1} at 30 °C (SD, n = 2,092 filaments, Fig. 3*B*) and 278 ± 36 nm·s^{-1} at 20 °C (SD, n = 1,712 filaments, Fig. 3*B*). Filament velocities were only slightly reduced (∼12%) in the presence of either 0.1 mM free

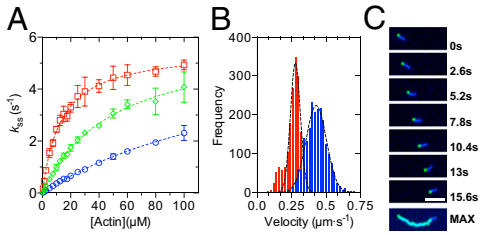

Fig. 3. Myosin 15 is an actin-activated ATPase with barbed-end–directed motility. (*A*) Steady-state ATPase activation of EGFP-Myo15-2IQ by actin filaments at 20 °C. At 100 mM KCl, $k_{cat} = 6.0 \pm 0.5\ s^{-1}$ and $K_{ATPase} = 164.6 \pm 18.9$ μM (mean ± SEM). The apparent affinity for actin (K_{ATPase}) was sensitive to salt concentration, whereas k_{cat} was not. Data points are mean ± SD from three preparations, [KCl]: 10 mM (red), 50 mM (green), 100 mM (blue). Basal ATPase activity was subtracted from each data point. (*B*) Histogram of actin filament velocities in a Myo15-2IQ-EGFP gliding assay. The average filament velocity was 429 ± 74 nm·s^{-1} at 30 °C (blue bars, n = 2,092 filaments from three preparations, mean ± SD, $R^2 = 0.985$) and 278 ± 36 nm·s^{-1} at 20 °C (red bars, n = 1,712 filaments from one preparation, mean ± SD, $R^2 = 0.952$). Gaussian fits are overlaid (dotted lines). (*C*) Montage of images from a time-lapse series of motile polarity-marked actin filaments using TIRF microscopy at 30 °C. Actin filaments were polymerized from TRITC-gelsolin seeds (green) and stabilized using Alexa 647-phalloidin (blue). A maximum projection (MAX) of the time-lapse stack shows the gelsolin-capped barbed-end trailing at the rear of the actin filament. All observed filaments (n = 73) were barbed-end directed. (Scale bar, 5 μm.)

Ca^{2+} (379 ± 51 nm·s^{-1}, SD, n = 312 filaments) or 0.2 mM tissue-purified smooth muscle tropomyosin (380 ± 59 nm·s^{-1}, SD, n = 206 filaments) when assayed at 30 °C. To determine if Myo15-2IQ-EGFP was a barbed or pointed-end–directed motor, we repeated the gliding assay using polarity-marked actin filaments that were polymerized from TRITC-labeled gelsolin seeds and recorded motility using total internal reflection fluorescence microscopy. All marked filaments moved with the fluorescently labeled barbed-end trailing, indicating that myosin 15 was barbed-end directed (Fig. 3*C*).

Single Molecule Measurements of Actin Interactions Show That Myosin 15 Is a High-Duty Ratio Motor. We measured the power stroke of single molecules of Myo15-2IQ-EGFP using the "three-bead" assay in a dual-beam optical trap (18). Myo15-2IQ-EGFP was stereo-specifically adsorbed onto pedestals using a single chain GFP-nanotrap that was used to prevent artificial dimerization through the IgG heavy chain. In the presence of saturating ATP (2 mM), we observed intermittent interactions of Myo15-2IQ-EGFP with the actin filament, as expected for a monomeric motor (Fig. 4*A*). An ensemble of single molecule events were collected (n = 611 interactions) and used to extract both mechanical and kinetic parameters of the myosin 15 motor domain. A Gaussian function was fit to the power stroke displacement histogram to estimate an average power stroke of 7.9 ± 1.3 nm (SEM) (Fig. 4*B*), which was consistent with purified Myo15-2IQ-EGFP having a lever arm formed of two IQ motifs (19). In addition, we compiled a histogram of the duration of individual acto-myosin interactions (Fig. 4*C*). The distribution was well fit by a single exponential decay with a mean actin-attached lifetime, τ = 161 ± 13 ms (SEM, detachment rate constant = $1/\tau = 6.2 \pm 0.5\ s^{-1}$). The single-molecule detachment rate constant calculated here was similar to the maximum catalytic rate measured at steady state by the NADH assay, $k_{cat} = 6.0 \pm 0.5\ s^{-1}$ (Fig. 3*A*) and suggests that myosin 15 spends the majority of its catalytic cycle bound to actin. We conclude that myosin 15 is a high-duty ratio motor.

Discussion

Unconventional Myosin 15 Is a HSP90/UNC-45 Client Protein. Several lines of evidence indicate that UNC45B promoted folding of the myosin 15 motor domain. First, when coexpressed with ELC, RLC, and calmodulin, EGFP-Myo15-3IQ aggregated heavily and only trace quantities were isolated as soluble protein. Overexpression of both UNC45B and HSP90AA1 significantly increased the yield of soluble protein without changing the overall expression levels of EGFP-Myo15-3IQ, indicating a reduction in protein aggregation. Second, UNC45B copurified with EGFP-Myo15-3IQ, strongly suggesting a chaperone–client protein interaction. Combined, these data indicate that in addition to folding conventional muscle myosin (12, 13), UNC45B can transiently interact with and promote maturation of an unconventional myosin. Our data do not exclude a posttranslational role for UNC45B, reported for other UCS (UNC-45, Cro1, She4, Rng3) domains containing proteins, that includes dimerization (20) and promoting acto-myosin interactions (21, 22). However, we note that our final myosin 15 preparation was monomeric and catalytically active in the absence of UNC45B.

HSP90 and its cochaperone UNC-45 are both required for folding of the muscle myosin motor domain (12, 13). Although we overexpressed both chaperones in our study, Sf9 cells do express HSP90 endogenously and this may be sufficient to fold myosin 15 provided that UNC45B is supplied exogenously. Two UNC-45 paralogs exist in mammals: UNC45A is ubiquitously expressed, whereas UNC45B is restricted to skeletal and cardiac tissues (23). These isoforms are not redundant in vivo (23, 24) and catalyze folding of smooth muscle myosin with different efficacies (13), hinting at an optimal pairing between chaperone and myosin client. Future experiments will examine if UNC45A can also catalyze myosin 15 folding, and if so, whether the purified myosin has similar properties to those reported here. Whether myosin 15 also requires UNC-45 to fold in sensory hair cells remains unknown.

Several other classes of unconventional myosin are reported to interact with UCS domain-containing proteins (25, 26). We are now investigating whether individually tailored combinations of UNC-45 and HSP90 isoforms might optimize expression of other myosin heavy chains in Sf9 cells. For example, limited quantities of cardiac myosin have been purified from Sf9 cells (27, 28), but yields appear higher when purified from C2C12 cardiomyocytes (29), which provide a muscle-like environment (30), in addition to endogenously expressing UNC-45 (23). The presence of metastable folding intermediates during myosin maturation, in addition to the identity and abundance of endogenous chaperones, may explain why some myosins can be successfully expressed in Sf9 cells, whereas others purify poorly, or not at all.

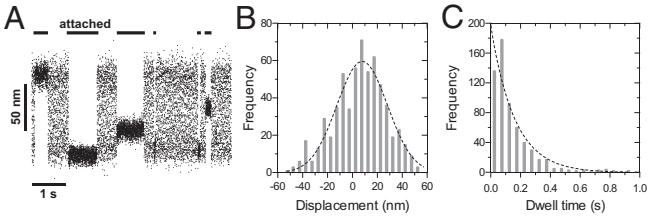

Fig. 4. Single molecule measurements of myosin 15 in the optical trap. (*A*) Sample records of single molecules of Myo15-2IQ-EGFP interacting with an actin filament in the three-bead assay at 23 ± 1 °C. Attached states (horizontal black bars) are detected as a reduction in the variance of bead motion, resulting from increased system stiffness as Myo15-2IQ-EGFP binds to the actin filament. No processive stepping events were observed. (*B*) Histogram of measured bead displacements in the three-bead assay. The distribution is offset from zero due to the myosin power stroke. A Gaussian fit (dotted line) estimates the power stroke = 7.9 ± 1.3 nm (n = 611 observations, four independent determinations, mean ± SEM, $R^2 = 0.897$). (*C*) Dwell time histogram of interactions with the actin filament. Fitting to a single exponential (dotted line) defines the detachment rate from actin, $k_{det} = 6.2 \pm 0.5\ s^{-1}$ (mean ± SEM, $R^2 = 0.925$).

We speculate that chaperone coexpression will help increase the quality and quantity of other purified myosin preparations. Increased yields are critical for kinetic, structural, and high-throughput studies, especially as myosins emerge as clinically important drug targets (31–33).

Light Chain Binding to Myosin 15. We show that the first two IQs of myosin 15 associate stably with smooth muscle RLC and ELC light chains, and that ELC can displace calmodulin from the second IQ domain. The expression of GFP-tagged RLC in cultured cells is a popular tool to report localization of nonmuscle myosin 2 isoforms (34, 35). Our finding that myosin 15 can bind RLC, similar to a recent report of myosin 18a (36) suggests that caution must be exercised in interpreting the results of GFP-RLC localization data. Although the endogenous light chains that associate with myosin 15 in vivo are unknown, RLC (MYL12B) and calmodulin (CALM) are both detected in the hair cell stereocilia proteome (37). Interestingly, calmodulin is highly concentrated at the stereocilia tips (38), and this may allow light chain exchange to occur as myosin 15 moves along the stereocilia core and enters the tip compartment. The association with RLC also raises the possibility that posttranslational modifications may regulate myosin 15. Phosphorylation of RLC at Ser19 activates the ATPase of smooth muscle heavy meromyosin (39); however, this involves relief of an autoinhibited dimeric state (40). One-headed smooth and nonmuscle myosin constructs are not regulated by phosphorylation (15, 41), and it is unclear, therefore, how phosphorylation might regulate a monomeric protein as reported here. RLC binding nearest to the converter domain of myosin 15, further suggests a different role to that reported for class II myosins.

Myosin 15 has a third potential light chain-binding domain (referred to as the third IQ here), which is highly divergent from the canonical IQ sequence (ΦQxxxRGxxxR), and did not bind calmodulin, ELC, or RLC under our experimental conditions. It remains to be seen whether this region can bind, an as-of-yet unidentified light chain, or whether it remains solvent exposed to potentially promote dimerization (42). Identification of the endogenous light chains in sensory hair cells will help understand how myosin 15 is regulated in vivo.

Functions of Myosin 15 Within Hair Cell Stereocilia. Our data show that myosin 15 is a barbed-end directed motor with a high-duty ratio at saturating [actin], i.e., spends a large proportion of its catalytic cycle attached to actin. Compared with other high-duty ratio motors, myosin 15 has a specificity constant (k_{cat}/K_{ATPase} = 0.12 $\mu M^{-1}\cdot s^{-1}$ at 50 mM KCl) that is an order of magnitude smaller than myosin 5a and 6 (11, 43). This difference is primarily due to a high K_{ATPase}, which in turn is interdependent upon the rates of actin-attached ADP release, phosphate release, and the equilibrium constant for ATP hydrolysis (11). The specific contribution of each of these reactions awaits a full characterization of the myosin 15 kinetic mechanism. Overall, the weak apparent affinity of myosin 15 for actin may be an adaptation for operating within hair cells, since stereocilia contain high concentrations of actin within the core paracrystal.

Our data suggest that full-length myosin 15 could undergo processive motility along stereocilia and filopodial actin filaments if the molecule was appropriately dimerized. No coiled-coil sequence is predicted to exist within myosin 15, and it remains unknown if dimerization occurs in vivo. Close apposition of the plasma membrane might alternatively allow myosin monomers to use diffusive sliding, biased by the power stroke, to ascend the uniformly polarized stereocilia actin filaments. There are no reported velocity estimates for myosin 15 moving along stereocilia or filopodia. Assuming that mouse cochlear stereocilia typically extend up to 5 μm, our data allow for simple predictions. If myosin 15 forms dimers, transit along the stereocilia core could be complete in ∼100 s (8-nm steps per turnover × 6 turnovers per second = ∼48 $nm\cdot s^{-1}$ at 20 °C). Actual velocities may differ considerably in vivo, due to increased catalytic activity at 37 °C. Additionally, the stereocilia actin core is complex, consisting of β and γ actins that are extensively decorated with actin-binding proteins (44). The recent demonstration that class V myosins in yeast are only processive on tropomyosin-associated actin filaments further highlights the importance of actin filament topology (45, 46). Future studies will address how myosin 15 interacts with different types of actin bundles, including the endogenous stereocilia substrate itself.

Existing data point to an additional role for myosin 15 within stereocilia. Ultrastructural studies show that myosin 15 accumulates adjacent to the lower tip-link insertion point in the stereocilia plasma membrane (47), a region that experiences significant tension during mechanotransduction (48). If membrane tension in this region were coupled to the stereocilia actin core via myosin 15, the motor domain could experience an oscillatory load up to several kilohertz. Force can fundamentally alter the mechanochemistry of myosin ATPases (49, 50), and it will be important to investigate how myosin 15 responds to dynamically varying loads of this type. The possibility that the myosin 15 power stroke might be reversible under oscillating high loads (51) is an exciting hypothesis to explain the apparent loss of fast adaptation in *Myo15*$^{sh2/sh2}$ inner hair cells (52).

Myosin 15 has a large tail domain in addition to the N-terminal extension, which likely serves to regulate and diversify motor function. We are particularly interested in how the N-terminal extension might modulate the motor activity of myosin 15. Recessive mutations in this large proline-rich domain are also associated with DFNB3 human deafness (4), yet its function within hair cells is unknown. Our work provides a foundation to now isolate full-length myosin 15 molecules. In doing so, we aim to develop quantitative biophysical models to understand how this critical sensory motor functions within hair cell stereocilia, and to ultimately provide a molecular understanding of DFNB3 deafness.

Materials and Methods

Expression and Purification of Myosin 15 from Sf9 Insect Cells. The motor and IQ light-chain binding domains of mouse myosin 15 (NP_874357.2) were fused to either an N- or C-terminal EGFP moiety. A C-terminal FLAG epitope (DYKDDDK) was included for affinity purification. Cloning and preparation of recombinant baculovirus is described in *SI Materials and Methods*. Sf9 cell cultures at 2 × 10^6 $cells\cdot mL^{-1}$ were synchronously infected with myosin 15, chaperone and light-chain viruses, each with a multiplicity of infection (MOI) of 5, and incubated with shaking (80 rpm) at 27 °C in HyClone SFX (GE Healthcare) supplemented with 2.5% (vol/vol) FBS and GlutaMAX (Life Technologies) for 48 h. Cell pellets were flash frozen in liquid N_2. Myosin 15 was purified as described in *SI Materials and Methods*.

Steady-State Assays. ATPase activity of EGFP-Myo15-2IQ (30 nM) was measured using a NADH coupled enzyme assay in the following buffer: 10 mM Mops (pH 7.0), 5 mM $MgCl_2$, 0.1 mM EGTA, (10–100 mM) KCl, 2 mM MgATP, 40 $units\cdot mL^{-1}$ lactate dehydrogenase, 200 $units\cdot mL^{-1}$ pyruvate kinase, 1 mM phosphoenolpyruvate, 200 μM NADH. The time course of NADH absorbance (A_{340}, ε = 6220 $M^{-1}\cdot cm^{-1}$) was followed using a spectrophotometer (UV-2450; Shimadzu) at 20 ± 0.1 °C and used to calculate the rate of ADP production.

In Vitro Motility Assays. Motility chamber preparation is detailed in *SI Materials and Methods*. Filaments were viewed in epifluorescence using an IX-51 inverted microscope (Olympus) and motility was recorded in the following buffer: 20 mM Mops (pH 7.0), 100 mM KCl, 5 mM $MgCl_2$ and 0.1 mM EGTA, 2 mM creatine phosphate, 50 mM DTT, 2 mM ATP, 3 mM glucose, 100 μM glucose oxidase, and 20 μM catalase at both 20 ± 0.5 °C and 30 ± 0.5 °C. Free Ca^{2+} (0.1 mM), or chicken gizzard tropomyosin (0.2 μM) was included as indicated. Actin filament velocities were analyzed as described previously (17). Polarity-labeled actin filaments (*SI Materials and Methods*) were visualized at 30 ± 0.5 °C using objective-type total internal reflection fluorescence microscopy on an Axiovert 200 M (Laser TIRF 3; Zeiss) sequentially excited with 561- and 647-nm light and captured using an EM-CCD camera (Evolve 512; Photometrics).

Optical Trapping. Three-bead assays were performed with a dual-beam optical trap apparatus using techniques previously described in detail (53–55). Preparation of assay chambers and purification of the GFP-nanotrap is described in *SI Materials and Methods*. All trapping experiments were at 23 ± 1 °C using an optical trap stiffness of 0.02–0.04 pN·nm^{-1} and the same buffer conditions as for the gliding assays above. A sinusoidal waveform (200 Hz; 100 nm peak to peak) was applied and the amplitude of the sinusoidal pickup used to monitor total system stiffness. Acto-myosin 15 attachments were detected as regions of reduced signal variance (53, 55).

ACKNOWLEDGMENTS. We thank Attila Nagy for the gift of pFastbac-EGFP-FLAG; Lisa Cunningham, Dennis Drayna, and Melanie Barzik for critical review of our manuscript; Earl Homsher and Sarah Heissler for helpful discussions; Ming Zhou and DaRue Prieto at the Advanced Technology Program (National Cancer Institute) for core proteomic services; and the Electron Microscopy Core Facility at the National Heart, Lung, and Blood Institute (NHLBI) for their support, advice, and use of facilities. This work was funded by the intramural funds of the NHLBI (HL004243-12 to J.R.S.) and the National Institute on Deafness and Other Communication Disorders (DC000039-17 to T.B.F.).

1. Belyantseva IA, Boger ET, Friedman TB (2003) Myosin XVa localizes to the tips of inner ear sensory cell stereocilia and is essential for staircase formation of the hair bundle. *Proc Natl Acad Sci USA* 100(24):13958–13963.
2. Liang Y, et al. (1999) Characterization of the human and mouse unconventional myosin XV genes responsible for hereditary deafness DFNB3 and shaker 2. *Genomics* 61(3):243–258.
3. Probst FJ, et al. (1998) Correction of deafness in shaker-2 mice by an unconventional myosin in a BAC transgene. *Science* 280(5368):1444–1447.
4. Nal N, et al. (2007) Mutational spectrum of MYO15A: The large N-terminal extension of myosin XVA is required for hearing. *Hum Mutat* 28(10):1014–1019.
5. Wang A, et al. (1998) Association of unconventional myosin MYO15 mutations with human nonsyndromic deafness DFNB3. *Science* 280(5368):1447–1451.
6. Belyantseva IA, et al. (2005) Myosin-XVa is required for tip localization of whirlin and differential elongation of hair-cell stereocilia. *Nat Cell Biol* 7(2):148–156.
7. Manor U, et al. (2011) Regulation of stereocilia length by myosin XVa and whirlin depends on the actin-regulatory protein Eps8. *Curr Biol* 21(2):167–172.
8. Berg JS, Powell BC, Cheney RE (2001) A millennial myosin census. *Mol Biol Cell* 12(4): 780–794.
9. Bloemink MJ, Geeves MA (2011) Shaking the myosin family tree: Biochemical kinetics defines four types of myosin motor. *Semin Cell Dev Biol* 22(9):961–967.
10. De La Cruz EM, Ostap EM (2004) Relating biochemistry and function in the myosin superfamily. *Curr Opin Cell Biol* 16(1):61–67.
11. De La Cruz EM, Wells AL, Sweeney HL, Ostap EM (2000) Actin and light chain isoform dependence of myosin V kinetics. *Biochemistry* 39(46):14196–14202.
12. Barral JM, Hutagalung AH, Brinker A, Hartl FU, Epstein HF (2002) Role of the myosin assembly protein UNC-45 as a molecular chaperone for myosin. *Science* 295(5555): 669–671.
13. Liu L, Srikakulam R, Winkelmann DA (2008) Unc45 activates Hsp90-dependent folding of the myosin motor domain. *J Biol Chem* 283(19):13185–13193.
14. Rayment I, et al. (1993) Three-dimensional structure of myosin subfragment-1: a molecular motor. *Science* 261(5117):50–58.
15. Cremo CR, Wang F, Facemyer K, Sellers JR (2001) Phosphorylation-dependent regulation is absent in a nonmuscle heavy meromyosin construct with one complete head and one head lacking the motor domain. *J Biol Chem* 276(44):41465–41472.
16. Kron SJ, Spudich JA (1986) Fluorescent actin filaments move on myosin fixed to a glass surface. *Proc Natl Acad Sci USA* 83(17):6272–6276.
17. Sellers JR, Cuda G, Wang F, Homsher E (1993) Myosin-specific adaptations of the motility assay. *Methods Cell Biol* 39:23–49.
18. Finer JT, Simmons RM, Spudich JA (1994) Single myosin molecule mechanics: piconewton forces and nanometre steps. *Nature* 368(6467):113–119.
19. Warshaw DM (2004) Lever arms and necks: A common mechanistic theme across the myosin superfamily. *J Muscle Res Cell Motil* 25(6):467–474.
20. Shi H, Blobel G (2010) UNC-45/CRO1/She4p (UCS) protein forms elongated dimer and joins two myosin heads near their actin binding region. *Proc Natl Acad Sci USA* 107(50):21382–21387.
21. Lord M, Pollard TD (2004) UCS protein Rng3p activates actin filament gliding by fission yeast myosin-II. *J Cell Biol* 167(2):315–325.
22. Lord M, Sladewski TE, Pollard TD (2008) Yeast UCS proteins promote actomyosin interactions and limit myosin turnover in cells. *Proc Natl Acad Sci USA* 105(23): 8014–8019.
23. Price MG, Landsverk ML, Barral JM, Epstein HF (2002) Two mammalian UNC-45 isoforms are related to distinct cytoskeletal and muscle-specific functions. *J Cell Sci* 115(Pt 21):4013–4023.
24. Comyn SA, Pilgrim D (2012) Lack of developmental redundancy between Unc45 proteins in zebrafish muscle development. *PLoS ONE* 7(11):e48861.
25. Hellerschmied D, Clausen T (2014) Myosin chaperones. *Curr Opin Struct Biol* 25:9–15.
26. Maliga Z, et al. (2013) A genomic toolkit to investigate kinesin and myosin motor function in cells. *Nat Cell Biol* 15(3):325–334.
27. Sata M, Ikebe M; Implication for the Clinical Outcome (1996) Functional analysis of the mutations in the human cardiac beta-myosin that are responsible for familial hypertrophic cardiomyopathy. Implication for the clinical outcome. *J Clin Invest* 98(12):2866–2873.
28. Sweeney HL, Straceski AJ, Leinwand LA, Tikunov BA, Faust L (1994) Heterologous expression of a cardiomyopathic myosin that is defective in its actin interaction. *J Biol Chem* 269(3):1603–1605.
29. Sommese RF, et al. (2013) Molecular consequences of the R453C hypertrophic cardiomyopathy mutation on human β-cardiac myosin motor function. *Proc Natl Acad Sci USA* 110(31):12607–12612.
30. Kinose F, Wang SX, Kidambi US, Moncman CL, Winkelmann DA (1996) Glycine 699 is pivotal for the motor activity of skeletal muscle myosin. *J Cell Biol* 134(4):895–909.
31. Bond LM, Tumbarello DA, Kendrick-Jones J, Buss F (2013) Small-molecule inhibitors of myosin proteins. *Future Med Chem* 5(1):41–52.
32. Malik FI, et al. (2011) Cardiac myosin activation: a potential therapeutic approach for systolic heart failure. *Science* 331(6023):1439–1443.
33. Straight AF, et al. (2003) Dissecting temporal and spatial control of cytokinesis with a myosin II Inhibitor. *Science* 299(5613):1743–1747.
34. Komatsu S, Yano T, Shibata M, Tuft RA, Ikebe M (2000) Effects of the regulatory light chain phosphorylation of myosin II on mitosis and cytokinesis of mammalian cells. *J Biol Chem* 275(44):34512–34520.
35. Peterson LJ, et al. (2004) Simultaneous stretching and contraction of stress fibers in vivo. *Mol Biol Cell* 15(7):3497–3508.
36. Guzik-Lendrum S, et al. (2013) Mammalian myosin-18A, a highly divergent myosin. *J Biol Chem* 288(13):9532–9548.
37. Shin JB, et al. (2013) Molecular architecture of the chick vestibular hair bundle. *Nat Neurosci* 16(3):365–374.
38. Shepherd GM, Barres BA, Corey DP (1989) "Bundle blot" purification and initial protein characterization of hair cell stereocilia. *Proc Natl Acad Sci USA* 86(13): 4973–4977.
39. Sellers JR, Pato MD, Adelstein RS (1981) Reversible phosphorylation of smooth muscle myosin, heavy meromyosin, and platelet myosin. *J Biol Chem* 256(24):13137–13142.
40. Wendt T, Taylor D, Messier T, Trybus KM, Taylor KA (1999) Visualization of head-head interactions in the inhibited state of smooth muscle myosin. *J Cell Biol* 147(7): 1385–1390.
41. Sweeney HL, Chen LQ, Trybus KM (2000) Regulation of asymmetric smooth muscle myosin II molecules. *J Biol Chem* 275(52):41273–41277.
42. Batters C, et al. (2014) Calmodulin regulates dimerization, motility, and lipid binding of Leishmania myosin XXI. *Proc Natl Acad Sci USA* 111(2):E227–E236.
43. De La Cruz EM, Ostap EM, Sweeney HL (2001) Kinetic mechanism and regulation of myosin VI. *J Biol Chem* 276(34):32373–32381.
44. Drummond MC, Belyantseva IA, Friderici KH, Friedman TB (2012) Actin in hair cells and hearing loss. *Hear Res* 288(1–2):89–99.
45. Clayton JE, et al. (2014) Fission yeast tropomyosin specifies directed transport of myosin-V along actin cables. *Mol Biol Cell* 25(1):66–75.
46. Hodges AR, et al. (2012) Tropomyosin is essential for processive movement of a class V myosin from budding yeast. *Curr Biol* 22(15):1410–1416.
47. Rzadzinska AK, Schneider ME, Davies C, Riordan GP, Kachar B (2004) An actin molecular treadmill and myosins maintain stereocilia functional architecture and self-renewal. *J Cell Biol* 164(6):887–897.
48. Assad JA, Shepherd GM, Corey DP (1991) Tip-link integrity and mechanical transduction in vertebrate hair cells. *Neuron* 7(6):985–994.
49. Laakso JM, Lewis JH, Shuman H, Ostap EM (2008) Myosin I can act as a molecular force sensor. *Science* 321(5885):133–136.
50. Veigel C, Molloy JE, Schmitz S, Kendrick-Jones J (2003) Load-dependent kinetics of force production by smooth muscle myosin measured with optical tweezers. *Nat Cell Biol* 5(11):980–986.
51. Sellers JR, Veigel C (2010) Direct observation of the myosin-Va power stroke and its reversal. *Nat Struct Mol Biol* 17(5):590–595.
52. Stepanyan R, Frolenkov GI (2009) Fast adaptation and Ca2+ sensitivity of the mechanotransducer require myosin-XVa in inner but not outer cochlear hair cells. *J Neurosci* 29(13):4023–4034.
53. Nagy A, et al. (2013) Kinetic characterization of nonmuscle myosin IIb at the single molecule level. *J Biol Chem* 288(1):709–722.
54. Takagi Y, et al. (2014) Myosin-10 produces its power-stroke in two phases and moves processively along a single actin filament under low load. *Proc Natl Acad Sci USA* 111(18):E1833–E1842.
55. Takagi Y, Homsher EE, Goldman YE, Shuman H (2006) Force generation in single conventional actomyosin complexes under high dynamic load. *Biophys J* 90(4): 1295–1307.